Powder Technology 203 (2010) 40–56

Contents lists available at ScienceDirect

Powder Technology

journal homepage: www.elsevier.com/locate/powtec

Computation and measurements of mass transfer and dispersion coefficients in fluidized beds

Mayank Kashyap, Dimitri Gidaspow *

Department of Chemical and Biological Engineering, Illinois Institute of Technology, Chicago, IL 60616, USA

ARTICLE INFO

Available online 9 April 2010

Keywords:
Dispersion coefficient
Mass transfer coefficient
Sherwood number
Circulating fluidized bed
Kinetic theory

ABSTRACT

Conventional design of circulating fluidized beds requires the knowledge of dispersion and mass transfer coefficients, expressed in dimensionless forms as Sherwood numbers. However, these are known to vary by five or more orders of magnitude. Furthermore, the Sherwood numbers for fine particles reported in the literature are several orders of magnitude lower than the Sherwood number of two for diffusion to a single particle. We have shown that by replacing the particle diameter in the conventional Sherwood number with cluster or bubble diameter, the modified Sherwood number is again of the order of two.

We have also shown that the kinetic theory based computational fluid dynamics codes correctly compute the dispersion and mass transfer coefficients. Hence, the kinetic theory based computational fluid dynamics codes can be used for fluidized bed reactor design without any such inputs.

1. Introduction

Conventional design of circulating fluidized beds, such as gasifiers [33], requires the knowledge of dispersion and mass transfer coefficients or Sherwood numbers. However, these are known to vary by five or more orders of magnitude [1].

We have recently shown that the particle and the gas axial and radial dispersion coefficients [18,19], and the mass transfer coefficients [3,4] can be computed using the kinetic theory based multiphase model, which is available in a commercial FLUENT code, the publically available MFIX [26] and in the IIT code [14].

2. Hydrodynamic model

The hydrodynamic model for the multiphase flow is based on the generalization of Navier–Stokes equations. The model numerically solved the set of governing conservation equations, mass, momentum, energy and species mass conservation, using the kinetic theory of granular flow [13]. The dense phase drag law was based on the Ergun equation, and the dilute drag law was a modification of Wen and Yu drag law [31,32]. However, to model the turbulent fluidization regime, the drag law was modified using the energy minimization principle [32]. Table 1 summarizes the kinetic theory based Hydrodynamic model A used in FLUENT. In the IIT code, the Hydrodynamic model B was used [16,17].

Fig. 1 shows that the dilute and the dense solid volume fractions of fluid cracking catalyst (FCC) particles can be computed using the modified drag model. We have conducted a similar study to that of Wei et al. [29] in the IIT two-story riser shown in Fig. 2. To obtain high fluxes, we have fluidized the downcomer. Fig. 3 shows our experimental data for FCC particles plotted on Matsen's phase diagram. Matsen's model is essentially the drift flux model reviewed by Gidaspow [13]. Recently, Gao et al. [12] also computed the two different volume fractions in the turbulent flow regime using the kinetic theory model in FLUENT, and compared the computations to experiments.

Fig. 4 shows that the model is able to resolve the spectral distribution of turbulence, beginning with the low frequency gravity wave down to the high frequency Kolmogorov regime.

We have also simulated the flow of cork particles in the NETL riser shown in Fig. 5. Fig. 6 shows that the pressure profile in the NETL riser with flow of cork is almost identical to the pressure distribution in the PRSI riser for flow of FCC particles when scaled with the density of the particles.

3. Computation of dispersion coefficients

Fig. 7 shows a comparison of the computed axial gas dispersion coefficient to literature correlations. Fig. 8 shows a similar computation for the radial gas dispersion coefficients. The radial gas dispersion coefficient is several orders of magnitude lower than the axial dispersion coefficient, as is well known in literature. Fig. 9 shows a comparison of the measured NETL cork axial solid dispersion coefficients to the CFD computation and the literature values. Fig. 10 shows a comparison of the computed radial solid dispersion

* Corresponding author.
E-mail address: gidaspow@iit.edu (D. Gidaspow).

0032-5910/$ – see front matter © 2010 Elsevier B.V. All rights reserved.
doi:10.1016/j.powtec.2010.03.025

Table 1
Kinetic theory based hydrodynamic model.

Conservation of mass or continuity equations

1. Gas phase:

$$\frac{\partial(\rho_g\varepsilon_g)}{\partial t} + \nabla\cdot(\rho_g\varepsilon_g v_g) = 0$$

2. Solid phase:

$$\frac{\partial(\rho_s\varepsilon_s)}{\partial t} + \nabla\cdot(\rho_s\varepsilon_s v_s) = 0$$

Conservation of momentum equations

1. Gas phase

$$\frac{\partial(\rho_g\varepsilon_g v_g)}{\partial t} + \nabla\cdot(\rho_g\varepsilon_g v_g v_g) = -\varepsilon_g\nabla P + \nabla\cdot\overline{\overline{\tau}}_g - \beta_A(v_g - v_s) + \varepsilon_g\rho_g g + \dot{m}_g\tilde{v}_g$$

2. Solid phase

$$\frac{\partial(\rho_s\varepsilon_s v_s)}{\partial t} + \nabla\cdot(\rho_s\varepsilon_s v_s v_s) = -\varepsilon_s\nabla P - \nabla P_s + \nabla\cdot\overline{\overline{\tau}}_s + \beta_A(v_g - v_s) + \varepsilon_s(\rho_s - \rho_g)g + \dot{m}_s\tilde{v}_s \quad (3)$$

Conservation of fluctuating energy equation for particles ($\theta = 1/3\langle C^2\rangle$)

$$\frac{3}{2}\left[\frac{\partial}{\partial t}(\varepsilon_s\rho_s\theta) + \nabla\cdot(\varepsilon_s\rho_s v_s\theta)\right] = \left(-\nabla P_s\overline{\overline{I}} + \overline{\overline{\tau}}_s\right) : \nabla v_s + \nabla\cdot(\kappa_s\nabla\theta) - \gamma_s$$

Conservation of energy equations

1. Gas phase

$$\frac{\partial}{\partial t}(\varepsilon_g\rho_g h_g) + \nabla.(\varepsilon_g\rho_g v_g h_g) = -\varepsilon_g\frac{\partial p_g}{\partial t} + \tau_g : \nabla.v_g + S_g + Q_{sg}$$

with, $h_g = \int c_{pg}dT_g$

2. Solid phase

$$\frac{\partial}{\partial t}(\varepsilon_s\rho_s h_s) + \nabla.(\varepsilon_s\rho_s v_s h_s) = -\varepsilon_s\frac{\partial p_s}{\partial t} + \tau_s : \nabla.v_s + S_s + Q_{gs}$$

with, $h_s = \int c_{ps}dT_s$

Conservation of species equations ($I = O_3$, O_2 or N_2 (air))

$$\frac{\partial}{\partial t}(\varepsilon_g\rho_g y_i) + \nabla.(\varepsilon_g\rho_g v_g y_i) = r_i$$

Constitutive equations

1). Definitions

$$\varepsilon_g + \varepsilon_s = 1$$

2). Gas pressure

$$P_g = \rho_g RT_g$$

3). Stress tensor (i = gas or solid)

$$\overline{\overline{\tau}}_i = 2\mu_i\varepsilon_i\overline{\overline{D}}_i + \varepsilon_i(\lambda_i - \tfrac{2}{3}\mu_i)\mathrm{tr}\left(\overline{\overline{D}}_i\right)\overline{\overline{I}}$$

where,

$$\overline{\overline{D}}_i = \frac{1}{2}\left[\nabla v_i + (\nabla v_i)^T\right]$$

4). Solid phase pressure

$$P_s = \rho_s\varepsilon_s\theta[1 + 2(1+e)g_0\varepsilon_s]$$

5). Solid phase shear viscosity

$$\mu_s = \frac{10\rho_s d_p\sqrt{\pi\theta}}{96(1+e)g_0\varepsilon_s}\left[1 + \frac{4}{5}(1+e)g_0\varepsilon_s\right]^2 + \frac{4}{5}\varepsilon_s\rho_s d_p g_0(1+e)\sqrt{\frac{\theta}{\pi}}$$

6). Solid phase bulk viscosity

$$\lambda_s = \frac{4}{3}\varepsilon_s\rho_s d_s g_0(1+e)\sqrt{\frac{\theta}{\pi}}$$

where, g_0 is the radial distribution function and μ_{sdil} is the particle phase dilute viscosity.

$$g_0 = \left[1 - \left(\frac{\varepsilon_s}{\varepsilon_{s,max}}\right)^{1/3}\right]^{-1}$$

7). Collisional dissipation of solid fluctuation energy

$$\gamma_s = 3(1-e^2)\varepsilon_s^2\rho_s g_0\theta\left(\frac{4}{d_s}\sqrt{\frac{\theta}{\pi}} - \nabla\cdot v_s\right)$$

8). Granular conductivity of fluctuating energy ($q = -k\nabla\theta$)

$$\kappa_s = \frac{150\rho_s d_p\sqrt{\pi\theta}}{384(1+e)g_0}\left[1 + \frac{6}{5}(1+e)g_0\varepsilon_s\right]^2 + 2\varepsilon_s^2\rho_s d_p g_0(1+e)\sqrt{\frac{\theta}{\pi}}$$

9). Gas–solid drag coefficient

Normal drag:

for $\varepsilon_g < 0.8$ (based on the Ergun equation)

$$\beta_A = 150\frac{\varepsilon_s^2\mu_g}{\varepsilon_g d_p^2} + 1.75\frac{\rho_g\varepsilon_s}{d_p}|v_g - v_s|$$

for $\varepsilon_g \geq 0.8$ (based on the empirical correlation)

$$\beta_A = \frac{3}{4}C_d\frac{\rho_g\varepsilon_s\varepsilon_g|v_g - v_s|}{d_p}\varepsilon_g^{-2.65}$$

EMMS drag

for $\varepsilon_g < 0.74$

$$\beta_A = 150\frac{\varepsilon_s^2\mu_g}{\varepsilon_g d_p^2} + 1.75\frac{\rho_g\varepsilon_s}{d_p}|v_g - v_s|$$

for $\varepsilon_g \geq 0.74$

$$\beta_A = \frac{3}{4}C_d\frac{\rho_g\varepsilon_s\varepsilon_g|v_g - v_s|}{d_p}\omega(\varepsilon_g)$$

when, $0.74 \leq \varepsilon_g \leq 0.82$, $\omega(\varepsilon_g) = -0.5760 + \frac{0.0214}{4(\varepsilon_g - 0.7463)^2 + 0.0044}$

when, $0.82 \leq \varepsilon_g \leq 0.97$, $\omega(\varepsilon_g) = -0.0101 + \frac{0.0038}{4(\varepsilon_g - 0.7789)^2 + 0.0040}$

when, $\varepsilon_g > 0.97$, $\omega(\varepsilon_g) = -31.8295 + 32.8295\varepsilon_g$

with,

$$C_d = \frac{24}{Re_p}\left[1 + 0.15Re_p^{0.697}\right] \quad \text{for } Re_p < 1000$$

$$C_d = 0.44 \quad \text{for } Re_p > 1000$$

$$Re_p = \frac{\varepsilon_g\rho_g d_p|v_g - v_s|}{\mu_g}$$

Table 1 (*continued*)

Boundary conditions for particle phase [58]

1). Velocity

$$v_{s,w} = -\frac{6\mu_s\varepsilon_{s,max}}{\sqrt{3\pi}\phi\rho_s\varepsilon_s g_0\sqrt{\theta}}\frac{\partial v_{s,w}}{\partial n}$$

2). Granular Temperature

$$\theta_w = -\frac{\kappa_s\theta}{\gamma_{s,w}}\frac{\partial\theta_w}{\partial n} + \frac{\sqrt{3\pi}\phi\rho_s\varepsilon_s v_{s,slip}^2 g_0\theta^{3/2}}{6\varepsilon_{s,max}\gamma_{s,w}} \text{ where } \gamma_{s,w} = -\frac{\sqrt{3\pi}(1-e_w^2)\varepsilon_s\rho_s g_0\theta^{3/2}}{4\varepsilon_{s,max}}$$

Boundary conditions for gas phase

$$v_{x,w} = v_{y,w} = 0$$

coefficients for the cork particles to related measurements in the literature. The gas and the particle dispersion coefficients are close to each other. They are all local values. They vary with axial and radial positions. We have shown that the kinetic theory based hydrodynamic model is capable of computing all the dispersion coefficients with a reasonable comparison to the literature reported in the last half a century.

4. Measurement of dispersion coefficients in the IIT two-dimensional CFB

4.1. Experimental setup

A two-dimensional circulating fluidized bed (CFB) was constructed and modified at IIT, for the measurements of dispersion and mass transfer coefficients, with partial financial support from UOP and the U.S. Department of Energy.

4.2. Schematic diagram

Fig. 11(A) shows the schematic diagram of the two-dimensional circulating fluidized bed (CFB) at IIT. The inner walls of the riser section of the fluidized bed were constructed of 0.5 inch thick glass sheets to avoid sticking of FCC particles to the walls, due to electrostatics caused by abrasion. The inside dimensions of the fluidized bed were 2 inch depth by 12 inch width by 50.5 inch height. The glass section was enclosed within a 0.5 inch thick acrylic sheet framework. The downcomer section of the fluidized bed was fabricated of 0.5 inch thick acrylic sheets, with the inside dimensions as 2 inch depth by 12 inch width by 55 inch height. Fine 304 L

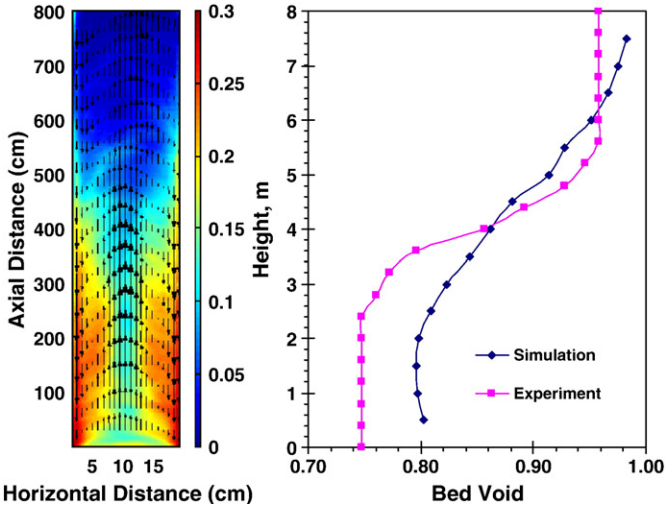

Fig. 1. Computed solid volume fraction structure in the Wei et al. [29] riser, showing turbulent flow regime [16].